4.3. Generating colloidal Fe/C composites *via* hydrothermal carbonization – a critical study

Maria Balda, Anett Georgi, Frank-Dieter Kopinke, Katrin Mackenzie

Department of Environmental Engineering, Helmholtz Centre for Environmental Research – UFZ, D-04318 Leipzig, Germany

Abstract: The aim of this work was to develop an approach for the bottom-up synthesis of colloidal Fe/C composites. It was tested whether the composites meet the main criteria for use as injectable adsorbents and reducing agents for the removal of chlorinated pollutants in *in-situ* groundwater remediation. After the screening of different Fe and C precursors, the bottom-up synthesis of a particulate and reactive Fe/C composite was developed *via* one-pot hydrothermal carbonization (HTC) of mixtures of ferrous and sodium gluconate and subsequent carbothermal reduction at 800 °C. The generated particles exhibit a good dispersibility with particle diameters in the range of $d_{10} \geq 2$ µm, $d_{50} \approx 11$ µm and $d_{90} \leq 40$ µm in aqueous suspensions. By varying the molar ratio of Fe to gluconate in the HTC process, the final content of zero-valent iron equivalents (ZVI) in the composite was adjusted between (24 ± 12) and (49 ± 15) wt.-%. The chemical reactivity of the composite was tested using reductive dechlorination of chloroform (CF). Characterization of the composites before and after reductive dechlorination with XRD indicates that not only pristine Fe^0 but also Fe_3C is active in the reductive dechlorination reaction. Palladization of the composite material shifts the product selectivity from dichloromethane as the main product to the non-chlorinated products methane (up to 77 mol-%) and ethane (up to 9 mol-%) without any external H_2 feed. The dispersiblity and intrinsic reactivity of the synthesized composites is favorable for the application in water remediation where contaminants need to be retained and degraded, *e.g.* for groundwater remediation or protection by the *in-situ* generation of permeable barriers using modern injection technologies.

Keywords: Fe/C composites; hydrothermal carbonization; dispersible; reductive dechlorination; chloroform; water remediation

1. Introduction

Water scarcity is a global problem, so it is important to safeguard the water quality of groundwater bodies in order to ensure high quality standards for drinking water. For this purpose, it is not only necessary to provide the required amount of water, *e.g.* by artificial groundwater recharge systems, but also to maintain and restore the desired water quality. However, the typically low concentrations of contaminants at polluted groundwater sites make effective remediation measures difficult. Therefore, innovative technologies combine adsorptive and reactive techniques to enrich the pollutants in the adsorbent phase and degrade them with an added reactant [2, 3]. The adsorbents and reactants used for remediation should be effective and cost-efficient while posing no additional threats to the treated water bodies. For this purpose, iron and carbon have proven to be suitable components due to their natural abundance, low price and non-toxic nature [4, 5]. Ideally, the degradation of the pollutant leads to the regeneration of the adsorptive function of the material. This combinatory approach has been established on the remediation market for *in-situ* groundwater remediation, *e.g.* Carbo-Iron® [6] or BOS 100® [7].

For the construction of permeable reactive zones by low-pressure injections into the aquifer, the adsorptive reagents should be quasi-dissolved and form sufficiently stable suspensions [8]. Particles with densities of about 1.1-2.6 g cm^{-3} ideally have diameters of about 1-2 µm in order to reach larger transport ranges [9, 10]. Nonetheless, it is also possible to inject larger particles, *e.g.* by stabilizing the suspensions in the form of biopolymer gels and applying higher injection pressures [11]. Beyond *in-situ* remediation, alike reactive adsorbents could also be useful in treating other water bodies where retention and degradation of pollutants are critical such as stormwater. For stormwater retention in urban areas for the local reuse and groundwater recharge such ‘enrich & treat’ options can help to prevent pollutants from reaching groundwater bodies *via* infiltration. Thus, there is a need to develop new materials or more sustainable synthesis ways for these kinds of remediation tasks.

The beneficial interaction of adsorptive and reactive material components of colloidal particles have been investigated with respect to environmental remediation, where highly selective and stable materials are required and contaminant concentrations are low, *e.g.* in groundwater remediation [12, 13]. The transfer of ‘chemical reactivity’ from ZVI to carbon was also demonstrated when both particles were in the suspended state,

even in the micro rather than the nano scale [14-17]. The corresponding transfer process of electrons or hydrogen species (H*) is referred to as spill-over.

In order to combine iron and carbon (Fe/C) in well-dispersible composite materials, usually multi-step synthesis approaches are used. The carbon material is pre-synthesized and then provided with the reactive component. In the case of iron, this is realized by wet impregnation of the carbon's pore system with iron salts and subsequent reduction [18]. In some cases, the reduction of oxidic iron on AC can be achieved with $NaBH_4$ [19]. Similar wet impregnation processes have also been reported for the preparation of Fe-containing composites using hydrochar instead of AC, where the (pre-pyrolyzed) hydrochar was soaked in a suspension containing iron salts and then thermally activated to produce porosity and form Fe particles [20, 21]. More recently, other processes have been investigated in which solid feedstocks were impregnated prior to hydrothermal treatment [22] or where the Fe was introduced into the hydrochar in particulate form, *e.g.* as magnetite *via* the co-precipitation method with $FeCl_2$ and $FeCl_3$ [23]. It should be noted, however, that when solid biomass or pre-synthesized (activated) carbons are used, the dispersibility and suitable particle sizes for low-pressure injections cannot be adjusted in a single synthesis step, but must be achieved either by separate synthesis of the carbonaceous precursor in the desired particle sizes [21] or through milling of either the precursor or the final composite [22-24].

An alternative to these multi-step syntheses described above is the one-pot synthesis of Fe/C composites, starting from dissolved precursors, preferably from renewable resources. There are already several studies dealing with the combination of iron and carbon within one step using hydrothermal carbonization (HTC). However, it has been shown that effectively combining iron and carbon in this manner is not trivial, as the iron precursors are typically hydrophilic and the carbonaceous phase formed is comparatively hydrophobic. In order to gain more insight into the possibilities and limitations of HTC-based bottom-up syntheses, particularly of colloidal Fe/C composites for *in-situ* application, the existing literature studies were comprehensively reviewed and evaluated.

1.1. State of knowledge on the bottom-up synthesis of colloidal Fe/C composites *via* HTC

In order to fabricate functional Fe/C composites as colloidal particles during HTC, in principal two different approaches are followed in literature: (I) HTC of freshly

synthesized Fe-containing NPs combined with sugar solutions (Table 1) and (II) HTC of fully dissolved Fe and C precursors (Table 2). Based on the objective of the present work, we focused on two criteria for our review, namely if the dispersibility of the composites was explicitly investigated and if the composites were tested regarding reductive dechlorination reactions.

Approach (I) typically led to Fe/C composites with particle diameters of 35-200 nm (cf. Table 1). This is due to the coating of the original particles and their aggregates with thin carbon shells of about 5-40 nm [25-27]. It seems that with this approach, Fe dominates the composite and the compatability with carbon is limited. For the planned *in-situ* application, the final ratio of Fe/C is crucial and should preferentially be adjusted between 10-30 wt.-% Fe. A sufficient proportion of C is needed to shield the magnetic attraction of ZVI, otherwise leading to excessive agglomeration of the particle during injection known from pure ZVI. For nZVI this has been identified as major limitation for the *in-situ* application [12, 28, 29]. Furthermore, approach (I) has the drawback that the Fe-containing NPs have to be synthesized individually, resulting in an additional step prior to HTC.

Table 1 Literature studies on the synthesis of colloidal Fe/C composites *via* HTC of solid Fe precursors and dissolved C precursors.

Ref.	Experimental	Result/Comments	Suggested Application(s)
Wang *et al.* [26]	• Oleic acid stabilized magnetite NPs (2.5 g L^{-1}) + glucose (0.6 M) in Teflon-sealed autoclave • HTC at 170 °C for 3 h	• Nanocomposites in the size range 100-200 nm • Fe_3O_4-NPs homogeneously distributed in the center of the carbon spheres (10 nm carbon shell) • Dispersible nanocomposites (Fe_3O_4/C) • No stability tests	Magnetic carrier (not tested)
Wei *et al.* [25]	• Freshly synthesized FeNi-NPs (0.5 g L^{-1}) + glucose (0.4 M) in Teflon®-sealed autoclave • HTC at 160 °C for 3.5 h/2.5 h	• Core-shell structured particles with 35 nm FeNi-core and 5-12 nm carbon shell • Composites dispersible in H_2O, EtOH and MeOH *via* ultrasonication • No stability tests	Magnetic carrier (not tested)

Bai *et al.* [30]	• Freshly synthesized Fe_3O_4-NPs (10 g L^{-1}) + glucose (0.5 M) mixed for 30 min and put in an autoclave • HTC at 160 °C for 8 h	• Core-shell particles of about 70 nm • Easily dispersible Fe_3O_4/C composites due to the hydrophilic C surface • No stability tests	Solid-phase extractant (tested for PAHs)
Zhang *et al.* [31]	• Freshly synthesized Fe_3O_4-NPs (5 g L^{-1}) + glucose (0.5 M) ultrasonicated for 20 min and put in a Teflon®-lined autoclave • HTC at 180 °C for 4 h	• Agglomerates of Fe_3O_4-NPs (primary particle size 10 nm) are coated with carbon • Hydrophilic C shell of Fe_3O_4 ameliorates dispersibility in H_2O • No stability tests	Solid-phase extractant (tested for PAHs)
Yang *et al.* [27]	• Freshly synthesized Fe_3O_4-NPs (6.7 g L^{-1}) + glucose (0.5 M) • HTC at 180 °C for 4 h	• Core-shell particles with an Fe_3O_4 core (70-80 nm) and a carbon shell (30-40 nm) • Overall diameter 100-120 nm Fe_3O_4/C dispersible *via* ultrasonication • No tests of suspension stability	Solid-phase extractant (tested for PAHs)

The literature studies that investigated approach (II) can be divided into two categories with respect to their results: the composite particles had diameters of either a few micrometers or below 100 nm, depending on the ratio of Fe to C precursor and additives (cf. Table 2). When moderate concentrations of glucose (about 0.5 M) were mixed with 0.05-0.15 M Fe salts, the excess of C precursor together with the catalyzing effect of Fe during the HTC process generated particle sizes of the carbonaceous phase of 5-8 µm separately from Fe-NPs [32-34]. In contrast, when the glucose concentrations were decreased to 0.17-0.25 M and combined with 0.06-0.2 M of Fe precursor, true composites were formed which exclusively consisted of Fe-NPs coated with thin carbon shells. Presumably, the deficit of C precursor led to an increased Fe content of the resulting composites which thus feature the typical behavior of nano-sized Fe-containing particles [35, 36]. Similarly sized composites were generated *via* HTC of more complex sugar-containing solutions such as olive mill wastewater [37, 38] and hydrolysates derived from pinewood chips [39]. These substrates contain phenols which can act as chelating agents for Fe. Correcher *et al.* studied the influence of gallic acid as a model chelating agent on the HTC of glucose and $Fe(NO_3)_3$ solutions

[35]. Their results suggest that the addition of chelating agents that do not carbonize themselves leads to a smaller particle size, higher Fe content and Fe-NP-like properties. For our planned application, we are aiming for composites with higher C contents in order to receive the favorable properties of a porous C phase with regard to local enrichment of pollutants and enhanced reactivity of the Fe phase [17, 40]. Gluconate, as used by *Luo et al.*, could be a compromise between a complexing agent and a C precursor that is able to carbonize in the presence of Fe [1]. An advantage might be that the Fe content of the resulting product can be adjusted more freely compared to the other synthesis methods. It is worth noting that approach (II) with dissolved iron salts gives rise to iron oxide particles rather than ZVI because HTC conditions are not strongly reducing. Reactivity for reduction processes (*e.g.* dechlorination) has to be implemented in a subsequent treatment step such as pyrolysis (carbothermal reduction: $FeO_x + C \rightarrow Fe^0 + CO_x$).

Table 2 Literature studies on the synthesis of colloidal Fe/C composites *via* HTC with dissolved Fe and C precursors.

Ref.	Experimental	Result/Comments	Planned Application(s)
Xuan *et al.* [36]	• Glucose (0.25 M), $FeCl_3$ (0.15 M) + urea (2.5 M) in water • HTC at 180 °C for 14 h	• Well-dispersed particles (100-200 nm diameter) • Carbon shell and single crystalline Fe_3O_4 core	Magnetic carrier (not tested)
Luo *et al.* [1]	• $FeCl_3$ (0.05 M) + sodium gluconate (0.15 M) in water • HTC at 180 °C for 48 h	• Dispersible and spherical Fe/C composites with multiple Fe_3O_4 cores, coated with a carbonaceous phase	Reagent for photo-Fenton reaction (tested for the oxidation of methylene blue)
Sun *et al.* [33]	• Glucose (0.5 M), $Fe(NO_3)_3$ (0.1 M) • HTC at 180 °C for 18 h • Thermal treatment at 350, 550 or 750 °C for 2 h	• Carbonaceous spheres of about 6-8 µm decorated with Fe-NPs	Catalyst for the activation of peroxymono-sulfate (tested for the oxidation of phenol with sulfate radicals)

Yan *et al.* [39]	• $FeCl_2$ (0.2 M) dissolved in a sugar solution derived from the acid hydrolysis of pine wood chips • HTC at 160-180 °C for 8 h • Thermal treatment at 700 °C for 1 h	• Aggregates with diameters of a few microns consisting of spherical Fe-NPs coated with a thin carbon shell	Catalyst for Fischer-Tropsch synthesis (tested with biomass derived syngas)
Liang *et al.* [34]	• $Fe(NO_3)_3$ and glucose in a 1:6 molar ratio • pH adjusted to 2, 4, 6 or 8 • HTC at 180 °C for 12 h	• Depending on pH during HTC microspheres from approx. 2-10 µm decorated with dispersed or large aggregates of NPs	Reagent for photo-Fenton reaction (tested for the oxidation of Orange II)
Calderon *et al.* [38]	• $Fe(NO_3)_3$ (0.2 M) dissolved in olive mill wastewater • HTC at 180-275 °C for 0.5-18 h	• Aggregates with diameters of (130 ± 50) nm consisting of Fe-NPs with 4 nm diameter coated with 1 nm carbon shell	Adsorbent/Reagent for removal of heavy metals (tested for Cu, Zn, Cr, Ni, Cd)
Correcher *et al.* [35]	• Glucose (0.17 M), gallic acid (0.02-0.0.06 M) $Fe(NO_3)_3$ (0.06-0.09 M), pH adjustment to various starting pHs between 1 and 12 • HTC at 180 °C for 5 h	• Aggregates consisting of Fe-NPs with thin carbon shells	Catalyst for Fischer-Tropsch-synthesis
Munoz *et al.* [37]	• $Fe(NO_3)_3$ (0.2 M) dissolved in olive mill wastewater • HTC at 225 °C for 3 h • Thermal treatment at 800 °C for 3 h	• Aggregates with diameters of a few microns consisting of Fe-NPs with a carbon shell (30-50 nm composite diameters)	Adsorbent (tested for diclofenac, sulfamethoxazole, metronidazole)
Jiang *et al.* [32]	• Glucose (0.6 M), $FeCl_2$ (0.05 M), $FeCl_3$ (0.07 M) + Urea (0.8 M) in water • HTC at 200 °C for 10 h • Functionalization with sulfonic acid groups	• Carbonaceous spheres of about 5 µm with partially attached ‘clouds’ of Fe_3O_4-NPs in between the spheres	Adsorbent (tested for methylene blue)

1.2. Derived approach for the experimental study presented here

The goal of this work was to find a bottom-up synthesis of an Fe/C composite, *i.e.* starting from dissolved Fe and C precursors and combining them within one step. The composite material should be mechanically stable, have a small particle size (in the lower µm range) and colloidal properties, and provide reactivity for reductive dechlorination reactions. Starting from dissolved iron/carbon precursors, different one-pot processes were investigated and the resulting product morphologies were evaluated.

Carbothermal reduction/activation of the HTC-generated Fe/C composite was used to further process the most promising material obtained from HTC of iron and sodium gluconate for application. To date, there are no studies in the literature investigating colloidal Fe/C composites from one-pot HTC synthesis and carbothermal reduction for dechlorination reactions. Therefore, we characterized for the first time the colloidal properties of the HTC-derived Fe/C composites in aqueous suspensions and the reactivity of the synthesized composite with respect to reductive dechlorination, including XRD and XPS analyses of the fresh *vs.* spent composites. In addition, the Fe/C composites were palladized and the product selectivity regarding the chloroform (CF) degradation was monitored. The known change in the reaction mechanism of palladized ZVI-based materials from electron-driven reductive dechlorination (Fe/C) to hydrodechlorination (Pd/Fe/C) [41] led to a significant enhancement of the selectivity towards fully dechlorinated and hydrogenated products. The selectivity of Pd/Fe/C was compared with Pd/Carbo-Iron® and other typical Pd-containing catalyst materials (Pd/AC, Pd/ZVI, Pd/magnetite, Pd/Al_2O_3 and Pd-NPs). The effects of palladization were tested because Pd not only increases the reaction rate but also broadens the spectrum of degradable compounds. For example, ZVI alone is not capable of attacking chlorinated aromatics, but Pd/ZVI is [42]. We are aware that Pd can have some adverse health effects when exposure to dissolved Pd^{2+} occurs [43]. However, Pd on ZVI is usually very stable and does not tend to dissolve, as Pd is more noble than ZVI [44]. The use of Pd-containing materials has been demonstrated regarding *in-situ* purification of groundwater [45] and it might remain necessary to use them in the future at contaminated sites with challenging pollutants – always subject to country-specific regulations. The herein synthesized composites could potentially be applied for *in-situ* contaminant retention and degradation, *e.g.* in percolation systems or aquifers.

2. Materials and Methods

2.1. Chemicals

All chemicals were purchased in analytical grade or higher. The detailed information about chemicals used in the experiments and materials used as catalyst support can be found in the supporting information (SI) in Text S1.

2.2. Bottom-up synthesis of Fe/C

After the screening of different Fe and C precursors (cf. SI Text S2 and Figure S1), colloidal Fe/C composites were synthesized *via* HTC of ferrous gluconate dihydrate (30-60 g L^{-1}) at 180 °C for 24 h in the absence and in the presence of CMC (0.6-1.5 g L^{-1}, resulting in 1 wt.-% related to the combined weight of ferrous and sodium gluconate). In order to adjust the Fe/C ratio, different concentrations of sodium gluconate (0-120 g L^{-1}) were added to the reaction mixture. The native pH_0 values prior to HTC were 4.6 ± 0.1 for mixtures with molar ratios of $n_{Fe}/n_{gluconate}$ = 1/2 and 5.3 ± 0.1 for $n_{Fe}/n_{gluconate}$ = 1/10, respectively. In some cases, the pH_0 was adjusted with 1 M HCl or 1 M NaOH above or below the native values. The dark brown/black precipitates obtained after HTC were washed with de-ionized water, dried and pyrolyzed at 800 °C for 2 h under N_2 with a heating rate of 1 K min^{-1}, in order to (partially) reduce the iron oxide species in the composite to ZVI. The resulting Fe/C composites were characterized for their material properties as well as their reactivity in the dechlorination of chloroform (CF). In order to ameliorate the selectivity of the CF degradation to fully dechlorinated products, the composites were palladized and their dechlorination performance was compared with that of various other palladized catalysts.

2.3. Preparation of palladized catalyst materials

2.3.1. Pd/Fe/C

For palladization of the Fe/C as well as Carbo-Iron® colloids, the particles were dispersed in de-oxygenated and de-ionized water *via* 10 min of ultrasonic treatment after shaking for approximately 24 h. Afterwards, the appropriate amount of a stock solution of Pd(II) acetate ($Pd(CH_3COO)_2$) was added to achieve Pd contents of 1-4 wt.-%, the mixture was vigorously shaken by hand for 30 s and then placed onto a horizontal shaker for 30 min until the aqueous phase was completely colorless. The palladization took place *via* the redox reaction according to eq. (1):

$$Fe + Pd^{2+} \rightarrow Fe^{2+} + Pd \quad (1)$$

Afterwards, the composite was washed with de-oxygenated methanol and dried under N_2 atmosphere.

2.3.2. Pd/AC

A slightly modified method as previously reported by [46] was used to prepare Pd/AC. Pd ions were reduced with H_2. 10 g of AC ($d \approx 1$ µm) were suspended in 1 L deionized water, dispersed for 30 min in an ultrasonic bath and spiked with the calculated amount of $Pd(ac)_2$ stock solution resulting in a Pd content of 1 wt.-%. The mixture was vigorously shaken for 1 h and centrifuged to separate liquid and solids. The separated solids were suspended in 1 L de-ionized water and purged with H_2 (100 mL min^{-1}) for 1 h to ensure the complete reduction to Pd^0. The resulting catalyst was washed with de-ionized water and ethanol and then dried in an oven at 100 °C under N_2 overnight.

2.3.3. Pd/ZVI

For Pd/ZVI synthesis, Nanofer Star iron was used as the carrier material. 3 g of the commercial nZVI was suspended in de-ionized and de-oxygenated water, dispersed for 15 min in an ultrasonic bath and then spiked with the calculated amount of $Pd(ac)_2$ stock solution resulting in a Pd content of 1 wt.-%. The mixture was vigorously shaken for about 3 h to ensure the complete reduction of Pd^{2+} (de-colorization of the solution). The solid was washed with de-ionized water and ethanol and then dried under N_2 atmosphere. To exclude possibly formed free Pd-NPs, a magnet was used to exclusively separate Pd/ZVI from the mixture.

2.4. Dechlorination reactions

Dechlorination tests of CF were performed with all synthesized materials in 10 mM $NaHCO_3$ solution (pH = 8.5). For this, 25 mL solution was filled in a 55 mL vial and purged with N_2 for 20 min. 15-25 mg of composite material was added and the suspension including headspace was purged for another 10 min. The reaction system was pre-conditioned by shaking the mixture overnight. Afterwards, it was placed in an ultrasonic bath for 10 min, in order to ensure the dispersion of the particulate composite. The batches were then spiked with the according amount of acetonic stock solution of CF resulting in $c_{0,CF}$ = 10 mg L^{-1} in the aqueous reaction mixture. The progression of the reaction was checked by analyzing the educts and products *via* headspace sampling and gas chromatography coupled with mass spectrometry (GC/MS) or with a flame-ionization detector (FID, for light hydrocarbons).

For the comparison of various palladized materials, external H_2 supply was ensured by purging the reaction batches additionally with H_2 for 15 min before sealing them in an airtight way and starting the reaction by adding CF.

In order to compare the performance of the synthesized composites, product selectivities (S) towards fully dechlorinated products were determined, using eq. (2) where $Y_{C1,C2}$ is the amount of carbon in the respective products (CH_4, C_2H_4, C_2H_6) and X_{CHCl3} the amount of converted CF carbon. The extent of CF conversion was ≥ 90 mol-% for all monitored reactions.

$$S = \frac{Y_{C1,C2}}{X_{CHCl3}} \quad (2)$$

The kinetics of the CF degradation was evaluated according to a first-order model. This description is rather simplified as the reaction system is complex regarding three fractions of CF in equilibrium – adsorbed on the solid composite, dissolved in the aqueous phase and gasous in the batch headspace. Less than 20 % of the CF present in the reaction batches was adsorbed on the composite materials under the applied conditions. Due to the overlying processes of adsorption and reductive dechlorination of the CF with the Fe/C composites, the reaction kinetics was investigated based on product formation as the main products are not significantly adsorbed. Specifically, the total CF concentration at a certain reaction time c_t was estimated based on the molar concentrations of the volatile main products DCM, ethane and methane formed at that time t. Despite the complex reaction system, the linearized graphs were well fitted with eq. (3) (cf. Figure S3) and an observed rate constant k_{obs} was determined in order to describe the reaction rates of the monitored CF degradation.

$$\ln\left(c_{0,CF} - \sum c_{products,i} \cdot n_{carbon,i}\right) = -k_{obs} \cdot t + \ln(c_{0,CF}) \quad (3)$$

$c_{0,CF}$ is the initial molar concentration of CF and $c_{0,CF} - \Sigma c_{products,i} \cdot n_{carbon,i}$ is the estimated CF concentration after certain reaction times. The number of carbon atoms $n_{carbon,i}$ in the products i takes into account the reaction stoichiometry.

For the comparison of ZVI reactivities, the observed rate constants were normalized to the mass concentrations of ZVI in suspension (c_{ZVI} [g L^{-1}], eq. (4)).

$$k_{norm} = \frac{k_{obs}}{c_{ZVI}} \quad (4)$$

For the comparison of the various palladized composite materials, a second-order rate constant expression was used: the specific catalytic activity A_{Pd} [L g^{-1} min^{-1}] according to eq. (5).

$$A_{Pd} = \frac{1}{c_{Pd} \cdot \tau_{1/2}} = \frac{k_{obs}}{c_{Pd} \cdot \ln(2)} \quad (5)$$

A_{Pd} is based on the applied concentration of palladium c_{Pd} [g L^{-1}] and the substrate half-life $\tau_{1/2}$ [min].

For the characterization of selected materials *via* XPS and XRD after palladization and after the reductive dechlorination of CF, the composites were washed with de-oxygenated water and methanol several times and dried at 80 °C under N_2. This approach was used to get an impression of the change of material components. We are aware that the state of the material during the reaction in aqueous media cannot be depicted by these analysis techniques.

2.5. Analysis methods

Microscopic images were recorded with a VHX digital microscope (Keyence).

The scanning electron microscopy (SEM) analyses were conducted with a Zeiss Merlin VP compact with a beam current of 250 pA and electron landing energy of 10 kV.

The particle diameters in aqueous suspension were analyzed with a Mastersizer 3000 (Malvern Panalytical). Samples were prepared by dispersing the Fe/C composites in 10 mM $NaHCO_3$ solution in the presence of CMC as stabilizing agent. The native pH (8.5 ± 0.3) of the suspensions was recorded with a pH meter (MP225, Mettler Toledo) equipped with a glass electrode (InLab® Micro, Mettler Toledo).

The specific surface area (*SSA*) was determined with a Belsorp MINI (BEL Japan). Adsorption/desorption of N_2 was performed at -196 °C after pretreatment of the samples under vacuum at 100 °C overnight. The obtained data were evaluated according to the BET theory.

In order to determine the reactive ZVI equivalents in the synthesized Fe/C composites (simplistically called 'ZVI' in the following text), 1 mL of half-concentrated HCl was added to 10 mg of the dry composites under inert atmosphere (V = 250 mL) and measuring the evolved H_2 with a GC-6850 (Agilent) coupled with a thermal conductivity detector (TCD) and a HP plot column.

The solid sample composition was explored by X-ray photoelectron spectroscopy (XPS, Kratos Ultra DLD) and X-ray diffraction (XRD, ULTIMA IV, Rigaku). The analyses parameters are described in detail in the SI (Text S5).

For the determination of dissolved chloride, aqueous samples were filtered by cellulose acetate filters (Ø 0.45 µm) and were analysed by ion chromatography (Dionex Integrion HPIC, Thermo Scientific).

GC/MS analyses were performed with a GCMS-QP2010 (Shimadzu) equipped with a DB-5ms column (Agilent) (30 m × 0.25 mm × 0.25 µm). Headspace samples (CF, DCM, monochloromethane) were injected at 200 °C with a column temperature of 60 °C and a He flow of 1 mL min^{-1}. The MS detector conditions were as follows: ion source at 250 °C, 70 eV, detection in the single-ion monitoring (SIM) mode.

Methane, ethane and ethene were measured with a GC-2010 plus (Shimadzu, GS-Q Plot column (Agilent)) coupled with an FID at an injection temperature of 200 °C and a column temperature of 60 °C. The quantification of the GC/MS and GC/FID analyses was based on external calibration with vials containing defined concentrations of CF/DCM and methane/ethane/ethene, respectively.

3. Results and Discussion

3.1. HTC of ferrous and sodium gluconate for generating colloidal Fe/C composites

After the screening of various Fe and C precursors (cf. SI, Text S2. And Figure S1), ferrous gluconate was chosen as precursor in order to benefit from the complexation of the Fe ions by gluconate during the early particle formation process under HTC conditions (cf. Figure 2). The final ZVI content of the composite was modified by the addition of sodium gluconate resulting in different molar ratios of Fe/gluconate ranging from 1/2 to 1/10. The HTC was performed in the presence and in the absence of CMC in order to investigate a possible influence of the stabilizing agent on the particle morphology [47]. The SEM images of the prepared samples are displayed in Figure S2. In principle, no significant differences between the samples were observed with digital microscopy. The SEM analysis (Figure 1) of the Fe/C composite shows rather small

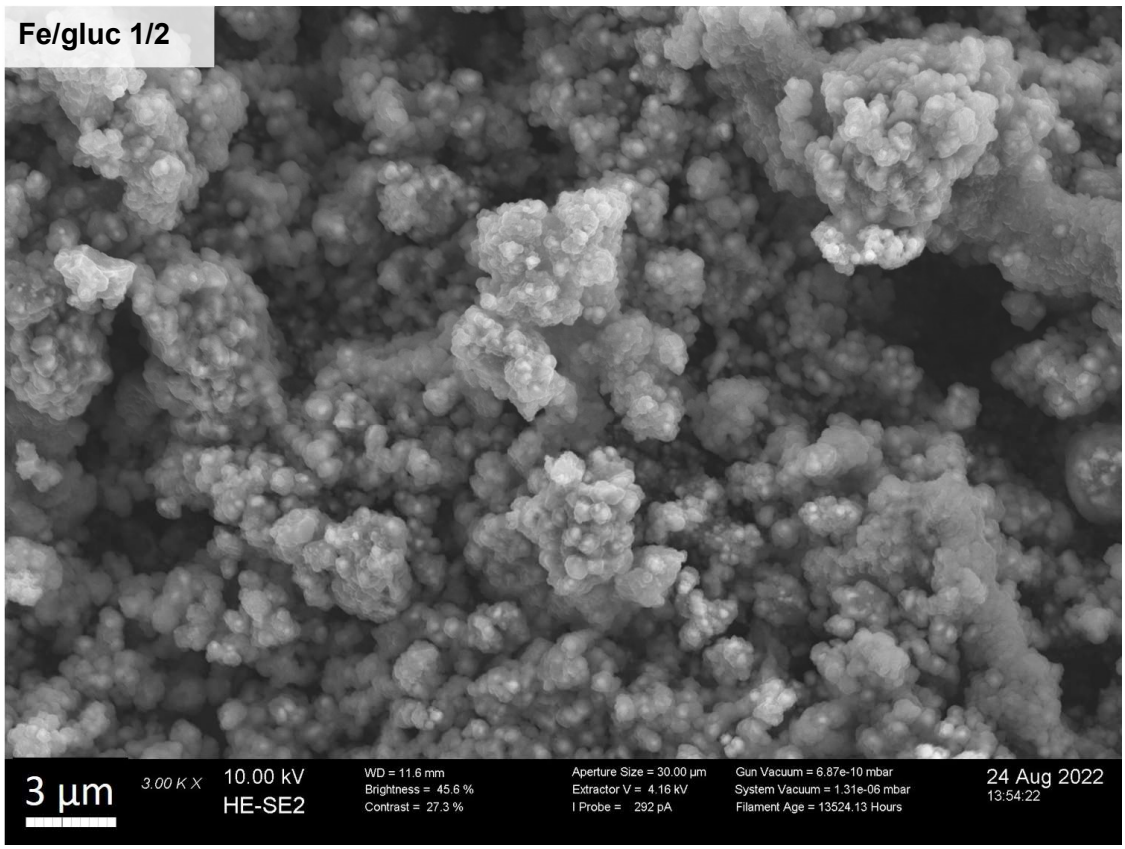

Figure 1 SEM image of the Fe/C composite synthesized *via* HTC of 120 g L^{-1} Na gluconate + 30 g L^{-1} Fe gluconate dihydate with subsequent carbothermal reduction at 800 °C under N_2.

and spherical primary particles. However, the effective particle size observed in aqueous suspensions was much larger (cf. Table 3), suggesting that the primary

particles become agglomerated during the hydrothermal synthesis and form aggregates of a few microns.

We assume that due to the formation of the $Fe^{2+/3+}$ gluconate complexes during synthesis the reaction system provides an inherent stability avoiding the disintegration of the two elements. However, a too low Fe concentration would lead to an insufficient carbonization of the C precursor, as gluconate alone does not carbonize into particles under the applied HTC conditions ($pH_{0,adjusted}$ = 5.3, 180 °C, 24 h). Due to its properties regarding the HTC process [48], the addition of Fe enables the carbonization of gluconate in our system. Typically, it is proposed that the promoting effect of iron acts mainly in the form of acidification and complexation with the organic matter formed [48]. Considering the growth mechanism proposed by Jung *et al*., the agglomeration of the initially formed nuclei is indeed a crucial step during the HTC process of soluble carbohydrates to enable particle growth [49]. However, in our case, we could rule out the sole pH effect because, as mentioned above, we did not observe any particle formation after the HTC of a sodium-gluconate solution that had been adjusted to the native pH of the ferrous gluconate solutions ($pH_0 \leq 5.3$). Therefore, we assume that the complexation of gluconate with ferrous/ferric ions might ensure local carbohydrate concentrations which are sufficiently high for enabling the intermolecular dehydration and polymerization reactions that lead to nucleation of the carbonaceous phase. Furthermore, it is assumed that the Fe ions not only ensure the complexation but might also participate in redox reactions [48, 50] that enable decarboxylation and dehydration reactions which are the initial steps during HTC processes. That is why we propose that a more homogeneous distribution of the Fe throughout the reaction mixture ensures a controlled carbonization process.

This effect might be most distinct when the Fe/gluconate molar ratio is 1/2 in order to ensure a complete complex formation throughout the reaction mixture. In Table 3 the

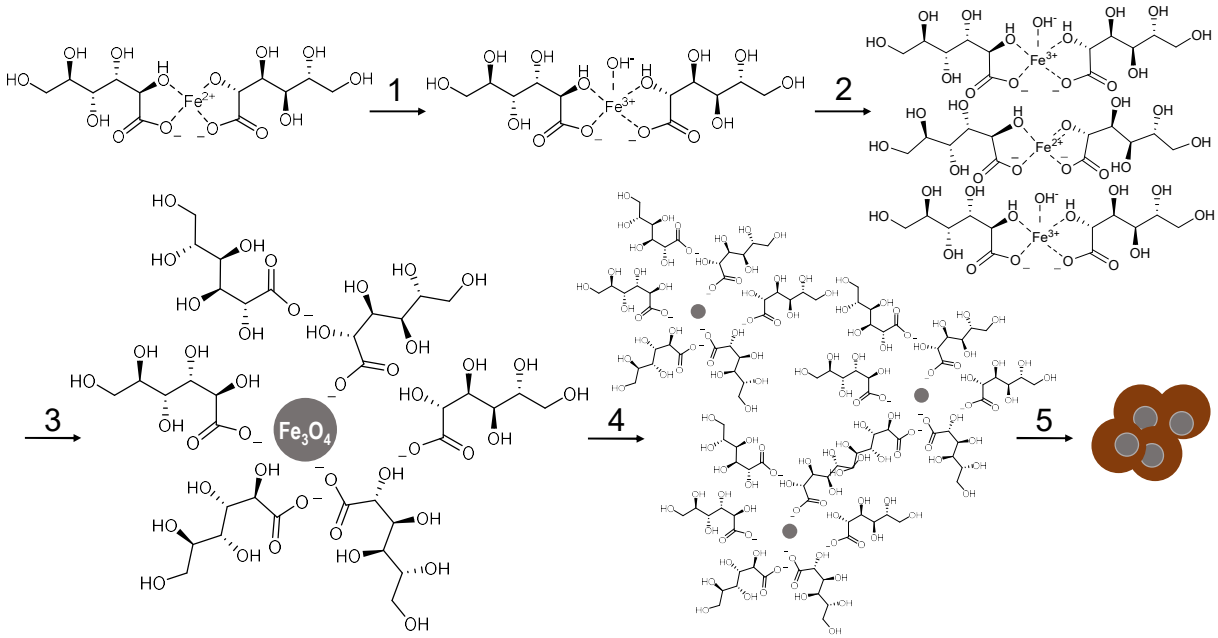

Figure 2 Proposed formation mechanism of Fe/C composites during the HTC of ferrous and sodium gluconate (scheme developed based on the proposed mechanism of [1]). The arrows represent simplified synthesis steps during the HTC process of ferrous gluconate: **1)** partial oxidation of Fe^{2+} to Fe^{3+}, **2)** assembly, **3)** formation of magnetite, **4)** coordination/agglomeration, **5)** formation of carbonaceous particles through dehydration, condensation, polymerization and aromatization reactions.

resulting ZVI contents of the samples with different molar Fe/gluconate ratios are displayed and ranged from (24 ± 12) to (49 ± 15) wt.-% after carbothermal reduction at 800 °C. Due to the necessity of Fe species for carbonization of the gluconate, it is anticipated that the ZVI contents of the resulting composites cannot be adjusted fully independently. Furthermore, the high variability of the lowest synthesized ZVI content of (24 ± 12) wt.-% in three replicate samples suggests a poorly controlled carbonization process presumably resulting in a more heterogeneous composite. Additionally, when the molar ratio of Fe/gluconate was decreased to 1/10, a decrease in the overall mass yield of composite particles down to (4 ± 1) wt.-% (related to the total mass of the introduced precursors Fe and gluconate) indicates in turn an incomplete carbonization of the sodium gluconate due to an iron deficiency. The mass yield was slightly increased and the deviation between replicates was decreased when 1 wt.-% CMC was added during the HTC compared to the synthesis in the absence of CMC. This could be due to the known stabilization effect of CMC which might reinforce a homogeneous distribution of the Fe throughout the reaction mixture and thus slightly enhancing the carbonization of gluconate. This assumption was tested with the HTC

of $n_{Fe}/n_{gluconate}$ = 1/2 in the presence of 2 wt.-% CMC (related to the combined weight of ferrous and sodium gluconate) where the char yield increased from 20 to 24 wt.-% after HTC (data not shown). However, the higher mass yield was accompanied by a loss of product homogeneity, confirming previous findings that small particle sizes and mass yields are a natural trade-off in HTC processes [47, 51].

Table 3 Characterization of Fe/C composites synthesized *via* HTC of ferrous and sodium gluconate and subsequent carbothermal reduction. Listing of ZVI contents (after carbothermal reduction), particle diameters in aqueous suspension (determined with dynamic light scattering), specific surface areas (SSA_{BET}) and mean pore diameters (d_{pore}) (both determined *via* N_2 ad/desorption) and their overall mass yields after carbothermal reduction. Note that the error ranges of the ZVI-contents, SSA_{BET}, d_{pore} and yield represent the mean deviation of single values from the mean value of at least two replicate synthesis experiments; the error ranges of the particle diameters represent the mean deviation of single values from the mean value of two measurements of the same sample.

n_{Fe} / $n_{gluconate}$	ZVI content [wt.-%]	Particle diameters [µm]			SSA_{BET} [m^2 g^{-1}]	d_{pore} [nm]	Yield [wt.-%]
		d_{10}	d_{50}	d_{90}			
1/10 + CMC	24 ± 12	2.2 ± 0.1	7.5 ± 0.3	31 ± 2	220 ± 50	6 ± 1	5 ± 1
1/5 + CMC	37 ± 5	n/d	n/d	n/d	150 ± 30	7 ± 1	9 ± 1
1/2 + CMC	42 ± 6	3.5 ± 0.1	12.6 ± 0.1	34.6 ± 0.4	140 ± 30	7 ± 1	11 ± 1
1/10	31 ± 4	3.4 ± 0.1	14.0 ± 0.1	36.2 ± 0.2	280 ± 60	4 ± 1	4 ± 1
1/5	34 ± 13	n/d	n/d	n/d	160 ± 40	7 ± 1	8 ± 2
1/2	49 ± 15	2.6 ± 0.1	9.2 ± 0.1	31.1 ± 0.1	160 ± 40	7 ± 1	10 ± 5

From Table 3 it can be seen that all synthesized composites provide broad particle size distributions from $d_{10} \geq 2$ to $d_{90} \leq 40$ µm in suspension. It is assumed that this is mostly due to agglomeration of the primary particles as a result of their ferromagnetic properties. The optimization of the resulting particle diameters towards a narrow size distribution in the range of a few µm was aspired but not achieved neither through the addition of CMC during the HTC process nor through the adjustment of initial pH values

(cf. Figure S3 and Text S4). Nevertheless, the suspension stability of the herein synthesized composites was effectively enhanced compared to nZVI particles (cf. Figure S10). Although the particle diameters of the composite material might be too large for low-pressure injections into aquifers or soils [52], injection techniques for micro-sized ZVI could be used in order to apply the material *in situ* [11].

In order to generate the desired reactivity for *in-situ* remediation, carbothermal reduction of the composites was necessary. During this pyrolysis process, the composites encountered a mass loss (46 ± 2) wt.-% enabling the formation of a porous structure. This resulted in overall mass yields of ≤ 10 wt.-% (related to the Fe and gluconate input) of the herein applied synthesis process. The influence of the pyrolysis step on the particle diameters in aqueous suspension was investigated regarding the composite synthesized at $n_{Fe}/n_{gluconate}$ = 1/10. After the HTC synthesis and prior to pyrolysis, the composite featured particle diameters ranging from $d_{10} \geq 4$ to $d_{90} \leq 80$ µm. Those were significantly reduced during the carbothermal reduction to $d_{10} \geq 3$ and $d_{90} \leq 35$ µm (cf. Table 3). This effect might on the one hand be rooted in the partial volatilization of the carbonaceous phase (decrease of oxygen content) due to pyrolysis and porosity generation. On the other hand, the Fe phase in the composite after HTC consists mainly of magnetite while, after carbothermal reduction, ZVI and Fe_3C are present (cf. Figure S6-S7). The latter exhibit different magnetic properties which may lead to less pronounced agglomeration effects.

The *SSA* of the composites were in the range of 140-280 $m^2\ g^{-1}$ with an increasing trend when the ZVI content was decreased. The resulting carbonaceous phase provided mean pore diameters in the mesopore range of about 4-7 nm. Regarding this, the samples differ from hydrochar which is pyrolyzed in the absence of iron where a strictly microporous system is developed [53, 54]. The increase in pore diameters results from the catalytic effect of iron oxides on the pyrolysis of carbon materials [55].

3.2. Reductive dechlorination of CF with the synthesized Fe/C composites

In order to test the accessibility and activity of the reactive iron in the composite for reductive dechlorination, CF was chosen as substrate. CF is a challenging target compound as its dechlorination proceeds *via* transfer of electrons or atomic hydrogen to DCM and methane as the two main products. Therefore, it not only allows to measure reaction kinetics of the reductive dechlorination but also the selectivities towards chlorinated and non-chlorinated products. The kinetic evaluation throughout

this work was performed according to the first-order model as shown for exemplary samples in Figure S4.

Table 4 Normalized rate constants k_{norm} of CF degradation (cf. eq. 4) and distribution of the main products methane and DCM at 90 % CF conversion in relation to $c_{0,CF}$ with various Fe/C composites synthesized by HTC and carbothermal reduction ($c_{0,CF}$ = 10 mg L^{-1}, $c_{Fe/C}$ = 400-1200 mg L^{-1}, 10 mM $NaHCO_3$, pH_0 = 8.5. The error ranges represent the mean deviation of single values from the mean value of two replicate experiments.

n_{Fe} / $n_{gluconate}$	ZVI-content [wt.-%]	k_{norm} [L g^{-1} h^{-1}]	Methane [mol-%]	DCM [mol-%]
1/10 + CMC	21 ± 1	0.04 ± 0.02	9 ± 2	72 ± 1
1/5 + CMC	39 ± 1	0.03 ± 0.01	10 ± 1	71 ± 1
1/2 + CMC	44 ± 6	0.017 ± 0.001	21 ± 3	48 ± 1
1/10	25 ± 2	0.023 ± 0.009	6 ± 1	60 ± 10
1/5	32 ± 1	0.020 ± 0.005	12 ± 2	62 ± 2
1/2	48 ± 2	0.023 ± 0.004	13 ± 1	73 ± 3

Table 4 shows that all Fe/C samples provide mass-normalized rate coefficients of (3 ± 1) · 10^{-2} L g^{-1} h^{-1} which is one order of magnitude higher than the rate coefficients recently reported in [56]. DCM is the dominant reaction product. Only traces of monochloromethane (MCM), ethene and ethane were found in all monitored reactions. The formation of DCM is unfavorable with respect to remediation goals. DCM is hardly reactive towards further dechlorination with ZVI as reductant. Similar DCM yields were also observed for nZVI [41]. Thus, the Fe/C composites prepared in a one-pot HTC synthesis followed by carbothermal reduction are active in reductive dechlorination but show the same shortcomings for the dechlorination of chloro-methanes as nZVI. In contrast, reactions involving Cu or noble metal catalysts and H_2 or borohydride as reductants show higher selectivities towards non-chlorinated products [41].

Accordingly, in order to improve the product selectivities of the Fe/C materials, their palladization with (1.2 ± 0.5) or (3.6 ± 0.5) wt.-% Pd was carried out resulting in Pd/Fe/C composites which were characterized with SEM-EDX. The elemental

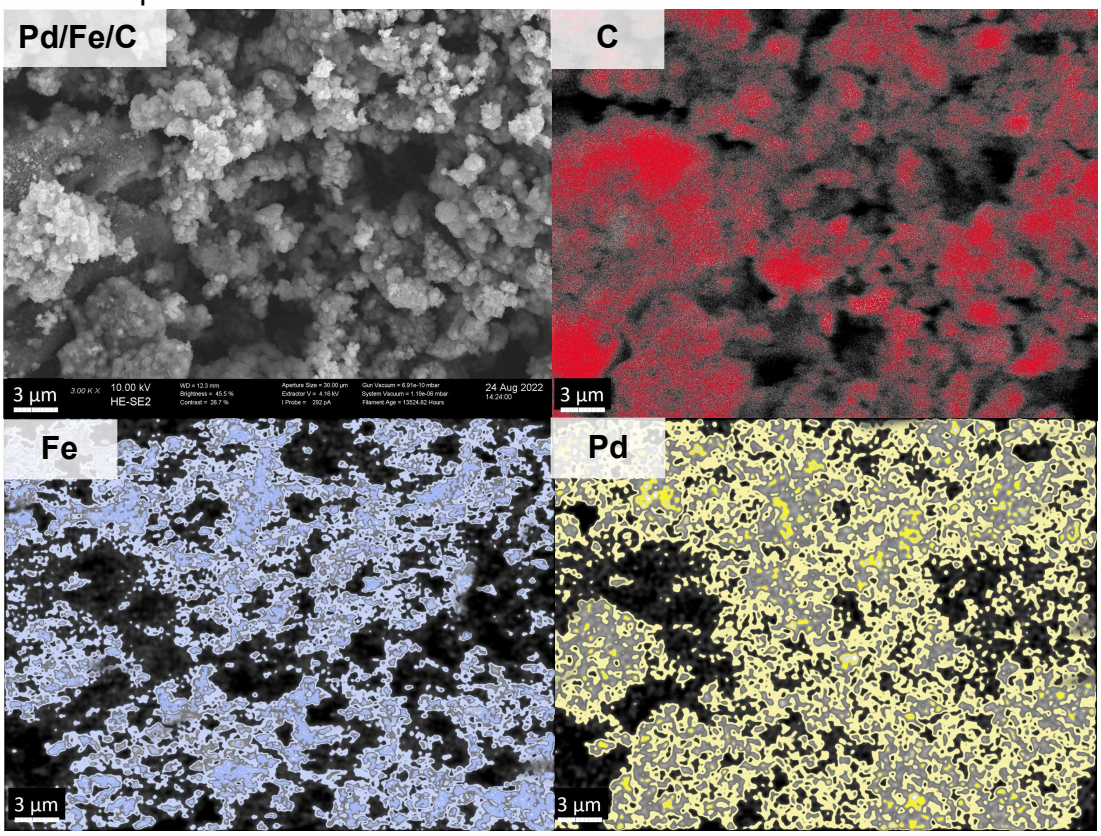

Figure 3 Elemental mapping with SEM/EDX analysis of a Pd/Fe/C composite containing ca. 30 wt.-% ZVI and 1 wt.-% Pd; C: red, Fe: blue, Pd: yellow.

mapping shown in Figure 3 reveals that Pd is deposited predominantly as distinct clusters on the Fe-rich sites, as expected.

After palladization, CF dechlorination activities were greatly enhanced. Furthermore, ethane was observed as additional product in significant amounts. When the samples were palladized with (1.2 ± 0.5) wt.-% Pd, significant gaps in carbon mass balances were observed which ranged from 20-40 mol-% (cf. Figure S5 and Tab. S2).

In order to investigate the reason behind these gaps, the CF degradation was performed with Pd/Fe/C (35 wt.-% ZVI and 1.5 wt.-% Pd) in a pure H_2 atmosphere (cf. Figure 4). The resulting rate constants and catalytic activities for the CF degradation

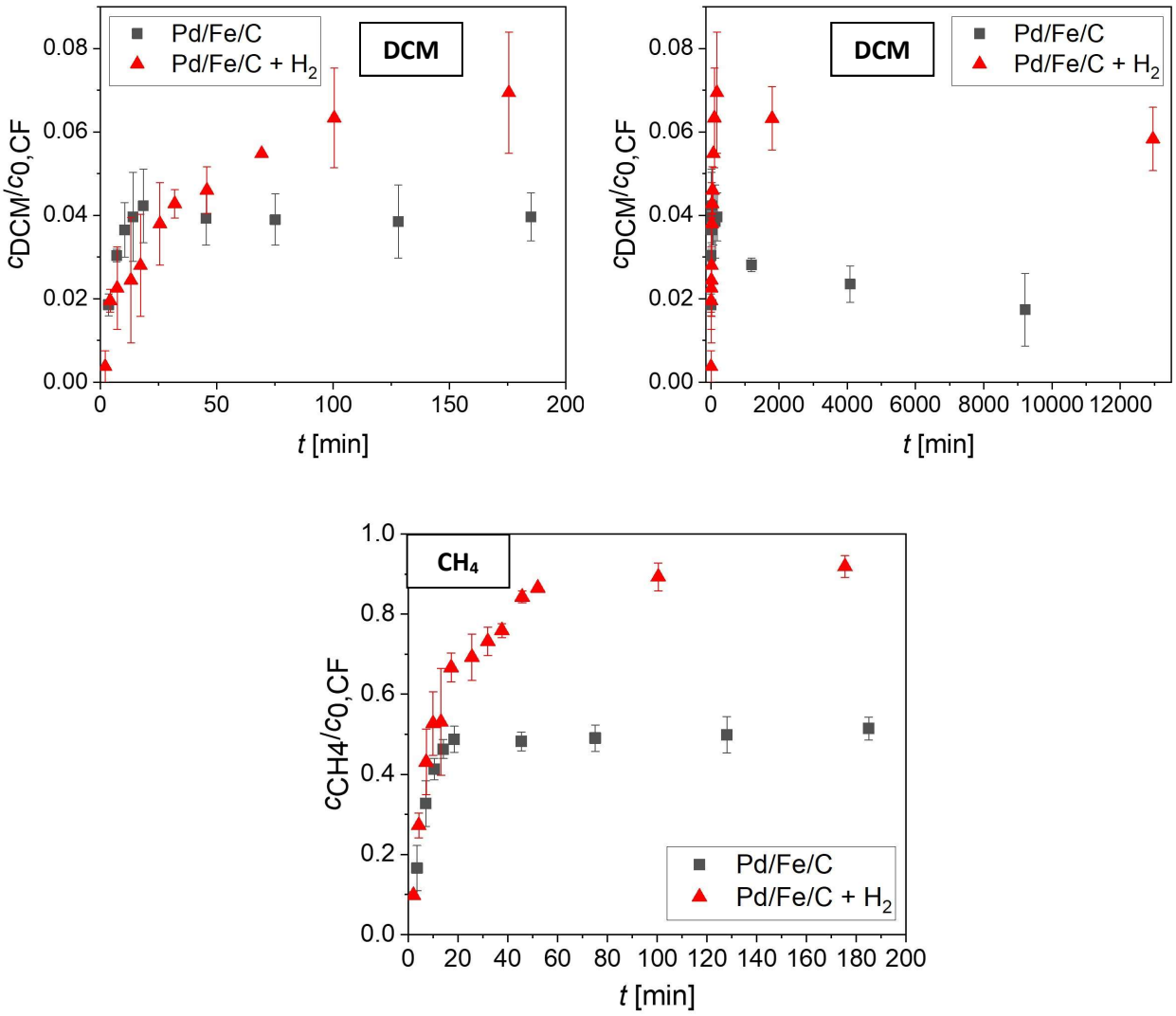

Figure 4 Formation of dichloromethane (DCM) and methane during reductive degradation of chloroform with Pd/Fe/C composites with 1.8 wt.-% Pd and 26 wt.-% ZVI under inert conditions and in H_2 atmosphere; note the different time scales in the two upper diagrams; the error bars represent the mean deviation of single values from the mean value of two replicate experiments.
$c_{0,CF}$= 7 mg L^{-1}, $c_{Pd/Fe/C}$ = 740 mg L^{-1}, c_{NaHCO3} = 10 mM, pH_0 = 8.5.

with Pd/Fe/C were essentially the same in the absence and in the presence of abundant H_2 (k_{norm} = (32 ± 7) L g^{-1} h^{-1} *vs.* (28 ± 4) L g^{-1} h^{-1} and A_{Pd} = (13 ± 3) L g^{-1} min^{-1} *vs.* A_{Pd} = (12 ± 2) L g^{-1} min^{-1}, respectively). This indicates that the availability of hydrogen is not rate limiting for the CF conversion, even with an initially inert gas atmosphere (N_2). This may be due to the fact that Pd is able to 'store' active hydrogen from the corrosion period prior to the reaction by chemisorption and make it available for CF degradation in the early reaction phase. However, with external H_2 supply, the

selectivity towards methane at > 99 % CF conversion was drastically enhanced from (51 ± 1) to (92 ± 1) mol-%. As the chloride yield with Pd/Fe/C ((87 ± 2) mol-%) was comparably high as the one with Pd/Fe/C + H_2 ((98 ± 5) mol-%), it is assumed that in both cases no excess amount of non-detected chlorinated byproducts besides DCM was formed. Instead, the observed propane formation led us to the assumption that radical-induced oligomerization processes take place [57, 58] which are obviously suppressed in the presence of abundant H_2 in the system. This assumption was strengthened by increasing the Pd content on the Pd/Fe/C samples to (3.6 ± 0.5) wt.-% Pd. At higher Pd contents and without external H_2 feed, the selectivities towards methane were increased up to 77 mol-% while the selectivities towards DCM were decreased to values as low as 2 mol.-% at > 95 % CF conversion (cf. Figure S5 and Text S4). This was attributed to an increase in anaerobic ZVI corrosion when more Pd was present due to the formation of local galvanic couples on the composite surfaces [59, 60]. Figure 4 reveals a slow but significant conversion of DCM with Pd/Fe/C in the absence and in the presence of external H_2. The comparison of k_{norm} of DCM and CF of around 0.02 L g^{-1} h^{-1} *vs.* around 30 L g^{-1} h^{-1} shows that DCM is significantly less reactive than CF. This is in line with relative reactivities of halogenated compounds in hydrodehalogenation reactions on Pd/Al_2O_3 as catalyst in aqueous media [61].

In order to gain more insight into the material composition, the samples Fe/C (1/10, 35 wt.-% ZVI) and Pd/Fe/C (1/10, 35 wt.-% ZVI and 1.1 wt.-% Pd) were characterized by XRD and XPS before and after the degradation of CF. The XRD spectra are displayed in the SI part (Figs. S6-S7). The crystalline structures of the Fe/C sample "1/10" consist mainly of Fe_3C (23 wt.-%), Fe^0 (15 wt.-%) and graphite (62 wt.-%) before the reaction. It should be noted that it was not analyzed to what extent the composite material is crystalline or amorphous. The formation of crystalline phases like iron carbide and graphite during the one-pot synthesis of Fe/C materials have been reported earlier for the HTC starting from the lignocellulosic matrix pinewood and iron(III) nitrate with subsequent calcination [62]. Gai *et al.* stated that the formation of iron carbide phases contributes to the mechanical stability of the composite material. Fe_3C as well as Fe^0 seem to be consumed during the CF degradation and the crystalline phases of the resulting composite consisted of magnetite (15 wt.-%) and graphite (85 wt.-%), suggesting that the Fe_3C phase might play a role in the reductive dechlorination of CF. This phenomenon was recently investigated by Meng *et al.* who

identified the potential of iron carbides to act as donor for electrons as well as atomic hydrogen (H*) in the reductive dechlorination of trichloroethene [63].

The crystalline phases of the synthesized Pd/Fe/C composite consisted of Fe_3C (18 wt.-%), Fe^0 (3 wt.-%), magnetite (21 wt.-%), graphite (46 wt.-%) and Pd (0.3 wt.-%) previous to the reaction. After the reaction, Fe^0 was absent and an increase in magnetite was observed (29 wt.-%). Graphite was depleted to 30 wt.-%. This might be due to conversion into amorphous carbonaceous species resulting in an overall decrease of the crystalline phase of the composite during the contact with water. This could explain why the Fe_3C content formally increased (36 wt.-%) in the crystalline phase of the composite. The Pd content stayed essentially the same (0.8 wt.-%), indicating the prevention of Pd leaching when in contact with Fe [44]. It is assumed that due to the preparation method of wet impregnation with Pd, Fe^0 was used up to some extent prior to the dechlorination and converted into magnetite. However, most of the Fe_3C remained and might enable the efficient hydrodechlorination in the presence of Pd resulting in a very active composite despite the low Fe^0 content. The significant decrease of the XRD signal intensities for both Fe/C and Pd/Fe/C after the reaction indicated that the crystalline phases were partially converted to more amorphous structures. The surface of the composite materials before and after reaction was characterized with XPS (cf. Figs. S8-S9). For Fe/C, the same trends as in the XRD analyses could be followed, namely an increase in surface oxygen content due to the consumption of Fe^0 and Fe_3C during the anaerobic corrosion in the aqueous phase. The binding energy of the most pronounced peak (C1s) at 284.5 eV indicated a state of mostly C=C double bonds which is in agreement with the graphite content verified by XRD. In the palladized samples, about 0.5 at.-% Pd were found on the surface.

Table 5 Specific catalytic activities A_{Pd} and product selectivities S of the CF dechlorination at 95 % conversion for various palladized materials; $c_{0,CF}$ = 10 mg L^{-1}, $c_{Pd/Fe/C,1/10}$ = 500 mg L^{-1}, $c_{Pd/Carbo\text{-}Iron}$ = 26 mg L^{-1}, $c_{Pd/AC}$ = 63 mg L^{-1}, $c_{Pd/magnetite}$ = 241 mg L^{-1}, $c_{Pd/Al2O3}$ = 766 mg L^{-1}, c_{NaHCO3} = 100 mM, pH_0 = 8.0-8.5, p_{H2} = 100 kPa. The error ranges represent the mean deviation of single values from the mean value of two replicate experiments.

	Pd-content	A_{Pd}	S [mol-%]			
Pd-catalysts	**[wt.-%]**	**[L g^{-1} min^{-1}]**	**methane**	**ethane**	**DCM**	**MCM**
Pd/Fe/C (w/o H_2)	4.0	9 ± 1	71	9.0	3.2	0.3
Pd/Fe/C	1.8	13 ± 1	85	3	6	0.6
Pd/Carbo-Iron®	1.1	190 ± 20	91.3	0.8	7.4	0.5
Pd/AC	0.8	40 ± 6	86	2.6	10	1.4
Pd-NP	100	20 ± 4	90.2	0.4	9.3	0.1
Pd/ZVI	0.8	1.4 ± 0.5	93.5	0.5	5.8	0.2
Pd/magnetite	0.2	10 ± 1	97.6	0.4	1.5	0.5
Pd/Al_2O_3	0.5	9 ± 1	94.4	0.3	5.5	< LOQ

The performance of Pd/Fe/C regarding the product selectivities (eq. (2)) and specific catalytic activities (eq. (6)) were compared with Pd/Carbo-Iron® as well as Pd/AC, Pd/ZVI, Pd/magnetite Pd/Al_2O_3 and Pd nanoparticles (cf. Table 5). It should be noted that in order to compare all catalyst materials without possible rate limiting H_2-formation steps, external H_2 was supplied (p_{H2} = 100 kPa). Under these conditions, methane was the main product with selectivities ≥ 85 mol-% for all investigated Pd-containing materials. Except of Pd/magnetite (with 1.5 mol-%), all investigated catalysts exhibited selectivities towards DCM of ≥ 5 mol-% increasing from Pd/Al_2O_3 (5.5 mol-%) < Pd/ZVI (5.8 mol-%) < Pd/Fe/C (6 mol-%) < Pd/Carbo-Iron® (7.4 mol-%) < Pd-NP (9.3 mol-%) and Pd/AC (10 mol-%). As the tested catalyst materials provided various particle sizes ranging from Pd-NPs (< 100 nm) to Pd/Al_2O_3 (25-63 µm), it has to be noted that the estimated catalytic activities can only be compared to some extent. The specific catalytic activity of Pd/Fe/C with external H_2 supply was in the same range as Pd/magnetite and Pd/Al_2O_3. In contrast, Pd/Carbo-Iron® featured the highest specific catalytic activity of (190 ± 20) L g^{-1} min^{-1} even though not having the lowest particle size and thus indicating the presence of most favorable Pd species. Presumably, the

higher SSA_{BET} of 720 $m^2\ g^{-1}$ and the well-dispersed ZVI-NPs on the surface may also lead to a more favorable Pd dispersion.

In this work, it was shown that the synthesized Pd/Fe/C composites degraded CF with a high chloride and low DCM yield even without external supply of H_2 but solely by intrinsic H_2 or H* from the anaerobic ZVI corrosion as required for *in-situ* remediation materials (cf. Figure S5). It is noteworthy, that for the reactions in the absence of external H_2, equally high selectivities towards non-chlorinated products and even a decrease of the selectivities towards the chlorinated by-products DCM and MCM could be achieved. However, this favorable effect was only observed at high Pd contents of up to 4 wt.-% (cf. Table 5 and S2) which was necessary to ensure a sufficient internal H_2 supply from enhanced ZVI corrosion. This would be certainly a matter of cost for individual applications. Furthermore, the increase in ZVI corrosion naturally leads to a faster ZVI depletion in the composite and thus limits the time of the availability of H_2 which is not favorable for *in-situ* applications where long-term activities of the applied reagents are desired [64]. Therefore, the palladized materials might only be suitable for urgent remediation measures over a short time-frame. Regarding the Fe/C material, longer life times are expected comparable to similar *in-situ* reagents which can even be extended by sulfidation of the material [65].

4. Conclusion

Bottom-up synthesis of a colloidal and reactive Fe/C composite was demonstrated based on the HTC of ferrous and sodium gluconate and a subsequent carbothermal reduction step with mass yields of ≤ 11 wt.-%, depending on the molar ratio of Fe/gluconate. The resulting Fe/C composites provide specific surface areas of 140-280 $m^2\ g^{-1}$ and a particle size distribution characterized by $d_{10} \geq 2$ µm, $d_{50} \approx 11$ µm and $d_{90} \leq 40$ µm. Thus, it can be concluded that the formation of dispersible Fe/C composites with uniform composition by a one-pot HTC process and subsequent carbothermal reduction is possible, but at the expense of a low mass yield and rather wide particle size distribution. The ZVI contents of the mechanically stable composites were adjusted from (24 ± 12) to (49 ± 15) wt.-%. The composite material was proven to provide reductive dechlorination activity as demonstrated for CF. However, the degradation reaction produced DCM as main product, showing as unfavorable selectivities as common ZVI-based reagents. The composite components of the synthesized Fe/C were characterized by XPS and XRD before and after the reaction,

suggesting that Fe_3C could be an additional active Fe species besides pristine Fe^0. Palladization of the composites resulted in faster CF degradation and a shift in selectivity towards fully dechlorinated reaction products without external H_2 feed. Compared to other typical catalyst supports, selectivities of Pd/Fe/C were favorable as the selectivities were higher towards ethane and lower towards DCM. In the presence of external H_2, the palladized Fe/C composites behaved similarly to Pd/AC in terms of selectivities and to Pd/magnetite and Pd/Al_2O_3 in terms of specific catalyst activities. The dispersibility with particle diameters below 50 µm, and mechanical stability of the synthesized composites could be advantageous for water treatment applications. However, despite considerable efforts, perfectly uniform composite particles in the size range suitable for low-pressure injection, *i.e.*, about 1 µm, could not be achieved. Nevertheless, the synthesized composites could be used *in-situ* with technologies that are already used for the application of µZVI or in percolation systems where adsorbents/reagents need to be added to retain and degrade contaminants. Future studies should therefore include additional reactivity testing in environmental media and long-term activity.

Acknowledgement: This study was funded by “Deutsche Forschungsgemeinschaft” (DFG), project number 392011053.

The authors thank Dr. Robert Köhler and Dr. Matthias Schmidt for the SEM analysis which was done at ProVIS – Centre for Chemical Microscopy at the UFZ, Leipzig, supported by European Regional Development Funds (EFRE-Europe funds Saxony) and the Helmholtz Association.

The authors are much obliged to Birgit Forkert and Wenbi Guan from the Department of Environmental Engineering (UFZ, Leipzig) for their experimental support by conducting the ion chromatography and BET analyses and performing additional dechlorination experiments. The authors acknowledge the laser diffraction analytics performed by ZetA Partikelanalytik GmbH, Mainz, under the direction of Dr. Andreas Hahn, and the XRD as well as the XPS measurements performed under the direction of Dr. Jan Griebel at the Institute of Surface Engineering (IOM), Leipzig.

References

[1] Z. Luo, H. Tang, L. Qu, T. Han, X. Wu, A visible-light-driven solid state photo-Fenton reagent basedon magnetite/carboxylate-rich carbon spheres, CrystEngComm 14 (2012) 5710-5713.

[2] H. Tang, D.Q. Zhu, T.L. Li, H.N. Kong, W. Chen, Reductive dechlorination of activated carbon-adsorbed trichloroethylene by zero-valent iron: carbon as electron shuttle, Journal of Environmental Quality 40(6) (2011) 1878-1885.
[3] K. Mackenzie, S. Bleyl, F.-D. Kopinke, H. Doose, J. Bruns, Carbo-Iron as improvement of the nanoiron technology: from laboratory design to the field test, Sci. Total Environm. 563-564 (2016) 641-648.
[4] S. Bleyl, F.-D. Kopinke, K. Mackenzie, Carbo-Iron® - synthesis and stabilization of Fe^0-doped colloidal activated carbon for in situ groundwater treatment, Chem. Eng. J. 191 (2012) 588-595.
[5] H. Choi, S. Agarwal, S.R. Al-Abed, Adsorption and simultaneous dechlorination of PCBs on GAC/Fe/Pd: mechanistic aspects and reactive capping barrier concept, Environ. Sci. Technol. 43(2) (2009) 488-493.
[6] Intrapore, CarboIron® - For the degradation of halogenated pollutants, 2023. (Accessed 20.08.2023 2023).
[7] R.P.I. RPI®, Safe & effective solutions: BOS 100, 2023. https://www.trapandtreat.com/products/. (Accessed 19.09.2023.
[8] T. Tosco, M.P. Papini, C.C. Viggi, R. Sethi, Nanoscale zerovalent iron particles for groundwater remediation: A review, Journal of Cleaner Production 15 (2014) 10-21.
[9] N. Tufenkji, M. Elimelech, Correlation equation for predicting single-collector efficiency in physicochemical filtration in saturated porous media, Environ. Sci. Technol. 38 (2004) 529-536.
[10] A. Georgi, J. Bosch, J. Bruns, K. Mackenzie, N. Saeidi, F.-D. Kopinke, Kolloidale Aktivkohle für die In-situ-Sanierung von PFAS-kontaminierten Grundwasserleitern, altlasten spektrum 6 (2020) 221-264.
[11] F. Mondino, A. Piscitello, C. Bianco, A. Gallo, A. Folly D'Auris, T. Tosco, M. Tagliabue, R. Sethi, Injection of Zerovalent Iron Gels for Aquifer Nanoremediation: Lab experiments and modeling, Water 12 (2020) 826-841.
[12] K. Pandey, S. Sharma, S. Saha, Advances in design and synthesis of stabilized zero-valent iron nanoparticles for groundwater remediation, J. Environ. Chem. Eng. 10 (2022) 107993.
[13] D. Fan, D.M. O'Carroll, D.W. Elliott, Z. Xiong, P.G. Tratnyek, R.L. Johnson, A.N. Garcia, Selectivity of nano zerovalent iron in *in situ* chemical reduction: challenges and improvements, Remediation 26 (2016) 27-40.
[14] F.-D. Kopinke, G. Speichert, K. Mackenzie, E. Hey-Hawkins, Reductive dechlorination in water: interplay of sorption and reactivity, Appl. Catal. B 181 (2016) 747-753.
[15] B.H. Tan, K.C. Tam, Y.C. Lam, C.B. Tan, Osmotic compressibility of soft colloidal systems, Langmuir 21 (2005) 4283-4290.
[16] F.-D. Kopinke, S. Suehnholz, A. Georgi, K. Mackenzie, Interaction of zero-valent iron and carbonaceous materials for reduction of DDT, Chemosphere 253 (2020) 126712.
[17] M. Vogel, F.-D. Kopinke, K. Mackenzie, Acceleration of microiron-based dechlorination in water by contact with fibrous activated carbon, Sci. Total Environm. 660 (2019) 1274-1282.
[18] K. Mackenzie, A. Schierz, A. Georgi, F.-D. Kopinke, Colloidal activated carbon and CARBO-IRON - Novel materials for in-situ groundwater treatment, Glob. NEST J. 10 (2008) 54-61.
[19] J. Zhan, I. Kolesnichenko, B. Sunkara, J. He, G.L. McPherson, G. Piringer, V.T. John, Multifunctional iron-carbon nanocomposites through an aerosol-based process for the *in situ* remediation of chlorinated hydrocarbons, Environ. Sci. Technol. 45 (2011) 1949-1954.
[20] Q. Ning, Y. Liu, S. Liu, L. Jaing, G. Zeng, Z. Zeng, X. Wang, J. Li, Z. Kare, Fabrication of hydrochar functionalized Fe-Mn binary oxide nanocomposites: characterization and 17β-estradiol removal, RSC Advances 7 (2017) 37122-37129.
[21] J. Zhan, B. Sunkara, L. Le, V.T. John, J. He, G.L. McPherson, G. Piringer, Y. Lu, Multifunctional colloidal particles for *in situ* remediation of chlorinated hydrocarbons, Environ. Sci. Technol. 43 (2009) 8616-8621.
[22] G. Davies, J. McGregor, Hydrothermal synthesis of biomass-derived magnetic carbon composites for adsorption and catalysis, ACS Omega 6 (2021) 33000-33009.

[23] F. Di Caprio, A. Pellini, R. Zanoni, M.L. Astolfi, P. Altimari, F. Pagnanelli, Two-phase synthesis of Fe-loaded hydrochar for As removal: The distinct effects of pH, reaction time and Fe/hydrochar ratio, J. Environ. Manage. 302 (2022) 114058.
[24] H. Takaesu, H. Matsui, Y. Nishimura, T. Matsushita, N. Shirasaki, Micro-milling super-fine powdered activated carbon decreases adsorption capacity by introducing oxygen/hydrogen-containing functional groups on carbon surface from water, Water Res. 155 (2019) 66-75.
[25] X.-W. Wei, G.-X. Zhu, C.-J. Xia, Y. Ye, A solution phase fabrication of magnetic nanoparticles encapsulated in carbon, Nanotechnology 17 (2006) 4307-4311.
[26] Z. Wang, H. Guo, Y. Yu, N. He, Synthesis and characterization of a novel magnetic carrier with its composition of Fe_3O_4/carbon using hydrothermal reaction, Journal of Magnetism and Magnetic Materials 302 (2006) 397-404.
[27] J. Yang, J.-Y. Li, J.-Q. Qian, H.-Z. Lian, H.-Y. Chen, Solid phase extraction of magnetic carbon doped Fe_3O_4 nanoparticles, Journal of Chromatography A 1325 (2014) 8-15.
[28] N. Saleh, H.J. Kim, T. Phenrat, K. Matyjaszewski, R.D. Tilton, G.V. Lowry, Ionic strength and composition affect the mobility of surface-modified Fe^0 nanoparticles in water-saturated sand columns, Environ. Sci. Technol. 42 (2008) 3349-3355.
[29] K. Mackenzie, A. Georgi, NZVI synthesis and characterization, in: T. Phenrat, G.V. Lowry (Eds.), Nanoscale zerovalent iron particles for environmental restoration, Springer International Publishing AG, Basel, 2019, pp. 45-95.
[30] L. Bai, B. Mei, Q.-Z. Guo, Z.-G. Shi, Y.-Q. Feng, Magnetic solid-phase extraction of hydrophobic analytes in environmental samples by a surface hydrophilic carbon-ferromagnetic nanocomposite, Journal of Chromatography A 1217 (2010) 7331-7336.
[31] S. Zhang, H. Niu, Z. Hu, Y. Cai, Y. Shi, Preparation of carbon coated Fe_3O_4 nanoparticles and their application for solid-phase extraction of polycyclic aromatic hydrocarbons from environmental water samples, Journal of Chromatography A 1217 (2010) 4757-4764.
[32] X. Jiang, Y. Jia, D. Ren, N. Zhang, T. Peng, Z. Huo, Magnetic seeds promoted high-density sulfonic acid-based hydrochar derived from sugar-rich wastewater for removal of methylene blue, Environ. Sci. Pollut. 30 (2022) 36872-36882.
[33] H. Sun, G. Zhou, S. Liu, H.M. Ang, M. O Tadé, S. Wang, Nano-Fe^0 encapsulated in microcarbon spheres: Synthesis, characterization and environmental applications, ACS Appl. Mater. Interfaces 4 (2012) 6235-6241.
[34] C. Liang, W. Zhao, Z. Song, S. Xing, Influence of precursor pH on the structure and photo-Fenton performance of Fe/hydrochar, RSC Advances 7 (2017) 35257-35264.
[35] R. Correcher, Y. Budyk, A. Fullana, Role of gallic acid in the synthesis of carbon-encapsulated iron nanoparticles by hydrothermal carbonization: Selecting iron oxide composition, ACS Omega 6 (2021) 29547-29554.
[36] S. Xuan, L. Hao, W. Jiang, X. Gong, Y. Hu, Z. Chen, A facile method to fabricate carbon-encapsulated Fe_3O_4 core/shell composites, Nanotechnology 18 (2007).
[37] M. Munoz, J. Nieto-Sandoval, S. Torrellas-Álvarez, E. Sanz-Santos, B. Calderón, Z.M. de Pedro, M. Larriba, A. Fullana, J. García, J.A. Casas, Carbon-encapsulated iron nanoparticles as reusable adsorbents for micropollutants removal from water, Sep. Purif. Technol. 257 (2021) 117974.
[38] B. Calderon, F. Smith, I. Aracil, A. Fullana, Green synthesis of thin shell carbon-encapsulated iron nanoparticles via hydrothermal carbonization, ACS Sustainable Chemistry & Engineering 6 (2018) 7995-8002.
[39] Q. Yan, J. Street, F. Yu, Synthesis of carbon-encapsulated iron nanoparticles from wood derived sugars by hydrothermal carbonization (HTC) and their application to convert bio-syngas into liquid hydrocarbons, Biomass Bioenerg. 83 (2015) 85-95.
[40] Z.G. Liu, F. Zhang, S.K. Hoekman, T.T. Liu, C. Gai, N.N. Peng, Homogeneously dispersed zerovalent iron nanoparticles supported on hydrochar-derived porous carbon: simple, *in situ* synthesis and use for dechlorination of PCBs, ACS Sustainable Chemistry & Engineering 4(6) (2016) 3261-3267.

[41] A. Shee, F.-D. Kopinke, K. Mackenzie, Borohydride and metallic copper as a robust dehalogenation system: Selectivity assessment and system optimization, Sci. Total Environm. 810 (2022) 152065.
[42] H. Hildebrand, K. Mackenzie, F.-D. Kopinke, Pd/Fe_2O_3 nano-catalysts for selective dehalogenation in wastewater treatment processes: Influence of water constituents, Appl. Catal. B 91 (2009) 389-396.
[43] J. Kielhorn, C. Melber, D. Keller, I. Mangelsdorf, Palladium - A review of exposure and effects to human health, Int. J. Hyg. Environ. Health 205 (2002) 417-432.
[44] D.W. Elliott, W.-X. Zhang, Field assessment of nanoscale bimetallic particles for groundwater treatment, Environ. Sci. Technol. 35 (2001) 4922-4926.
[45] F. He, D. Zhao, C. Paul, Field assessment of carboxymethyl cellulose stabilized iron for in situ destruction of chlorinated solvents, Water Res. 44 (2010) 2360-2370.
[46] H. Hildebrand, K. Mackenzie, F.-D. Kopinke, Highly active Pd-on-magnetite nanocatalysts for aqueous phase hydrodechlorination reactions, Environ. Sci. Technol. 43 (2009) 3254-3259.
[47] M. Balda, K. Mackenzie, F.-D. Kopinke, A. Georgi, Uniform and dispersible carbonaceous microspheres as quasi-liquid sorbent, Chemosphere (2022) 136079.
[48] V. Saadattalab, X. Wang, A.E. Szego, H. N., Effects of metal ions, metal and metal oxide particles on the synthesis of hydrochars, ACS Omega 5 (2020) 5601-5607.
[49] D. Jung, M. Zimmermann, A. Kruse, Hydrothermal carbonization of fructose: growth mechanism and kinetic model, ACS Sustainable Chemistry & Engineering 6 (2018) 13877-13887.
[50] A.M. Vindedahl, J.H. Strehlau, W.A. Arnold, R.L. Penn, Organic matter and iron oxide nanoparticles: aggregation, interactions and reactivity, Environmental Science: Nano 3 (2016) 494-505.
[51] M. Sevilla, A.B. Fuertes, Chemical and structural properties of carbonaceous products obtained by hydrothermal carbonization of saccharides, Chem. Eur. J. 15(16) (2009) 4195-4203.
[52] A. Georgi, A. Schierz, K. Mackenzie, F.-D. Kopinke, Colloidal activated carbon for *in-situ* groundwater remediation - Transport characteristics and adsorption of organic compounds in water-saturated sediment columns, Journal of Contaminant Hydrology 179 (2015) 76-88.
[53] L. Mao, Y. Zhang, Y. Hu, K.H. Ho, Q. Ke, H. Liu, Z. Hu, D. Zhao, J. Wang, Activation of sucrose-derived carbon spheres for high performance supercapacitor electrodes, RSC Advances 5 (2015) 9307-9313.
[54] M. Balda, K. Mackenzie, S. Woszidlo, H. Uhlig, J. Möllmer, F.-D. Kopinke, G. Schüürmann, A. Georgi, Bottom-up synthesis of de-functionalized and dispersible carbon spheres as colloidal adsorbent, Int. J. Mol. Sci. 24 (2023) 3831.
[55] M.B. Ahmed, J.L. Zhou, H.H. Ngo, W. Guo, M. Chen, Progress in the preparation and application of modified biochar for improved contaminant removal from water and wastewater, Bioresource Technology 214 (2016) 836-851.
[56] L. Gong, J. Chen, Y. Hu, K. He, E.J. Bylaska, P.G. Tratnyek, F. He, Degradation of chloroform by zerovalent iron: effect of mechanochemical sulfidation and nitridation on the kinetics and mechanism, Environ. Sci. Technol. 57 (2023) 9811-9821.
[57] J. Feng, T.T. Lim, Pathways and kinetics of carbon tetrachloride and chloroform reductions by nano-scale Fe and Fe/Ni particles: comparison with commercial micro-scale Fe and Zn, Chemosphere 59(9) (2005) 1267-1277.
[58] H.-L. Lien, S. Yuan-Pang, W.-X. Zhang, Nanoscale Bimetallic Pd/Fe particles for remediation of halogenated methanes, in: I.M.C. Lo, R.Y. Surampalli, K.C.K. Lai (Eds.), Zero-valent iron reactive materials for hazardous waste and inorganics removal2006.
[59] Y. Xu, W.-X. Zhang, Subcolloidal Fe/Ag particles for reductive dehalogenation of chlorinated benzenes, Ind. Eng. Chem. Res. 39 (2000) 2238-2244.
[60] K. Mondal, G. Jegadeesan, S.B. Lalvani, Removal of selenate by Fe an NiFe nanosized particles, Ind. Eng. Chem. Res. 43 (2004) 4922-4934.
[61] K. Mackenzie, H. Frenzel, F.-D. Kopinke, Hydrodehalogenation of halogenated hydrocarbons in water with Pd catalysts: Reaction rates and surface competition, Appl. Catal. B 63 (2006) 161-167.

[62] C. Gai, F. Zhang, Q. Lang, T. Liu, N. Peng, Z. Liu, Facile one-pot synthesis of iron nanoparticles immobilized into the porous hydrochar for catalytic decomposition of phenol, Appl. Catal. B 204 (2017) 566-576.
[63] F. Meng, Z. Li, C. Lei, K. Yang, D. Lin, Removal of trichloroethene by iron-based biochar from anaerobic water: key roles of Fe/C ratio and iron carbides, Chem. Eng. J. 413 (2021) 127391.
[64] A. Pavelková, V. Stejskal, O. Vološčuková, J. Nosek, Cost-effective remediation using microscale ZVI: comparison of commercially available products, Ecol. Chem. Eng. S. 27 (2020) 211-224.
[65] M. Vogel, A. Georgi, F.-D. Kopinke, K. Mackenzie, Sulfidation of ZVI/AC composite leads to highly corrosion-resistant nanoremediation particles with extended life-time, Sci. Total Environm. 665 (2019) 235-245.